

η' nucleus optical potential and possible η' bound states

H. Nagahiro, S. Hirenzaki

Department of Physics, Nara Women's University, Nara 630-8506, Japan

E. Oset

*Departamento de Física Teórica and IFIC,
Centro Mixto Universidad de Valencia-CSIC,
Institutos de Investigación de Paterna,
Apto. 22085, 46071 Valencia, Spain*

A. Ramos

*Departament d'Estructura i Constituents de la Matèria and Institut de Ciències del Cosmos.
Universitat de Barcelona, Avda. Diagonal 645, 08028 Barcelona, Spain
(Dated: July 29, 2021)*

Abstract

Starting from a recent model of the $\eta'N$ interaction, we evaluate the η' -nucleus optical potential, including the contribution of lowest order in density, $t\rho/2m_{\eta'}$, together with the second order terms accounting for η' absorption by two nucleons. We also calculate the formation cross section of the η' bound states from (π^+, p) reactions on nuclei. The η' -nucleus potential suffers from uncertainties tied to the poorly known $\eta'N$ interaction, which can be partially constrained by the experimental modulus of the $\eta'N$ scattering length and/or the recently measured transparency ratios in η' nuclear photoproduction. Assuming an attractive interaction and taking the claimed experimental value $|a_{\eta'N}| = 0.1$ fm, we obtain a η' optical potential in nuclear matter at saturation density of $V_{\eta'} = -(8.7 + 1.8i)$ MeV, not attractive enough to produce η' bound states in light nuclei. Larger values of the scattering length give rise to deeper optical potentials, with moderate enough imaginary parts. For a value $|a_{\eta'N}| = 0.3$ fm, which can still be considered to lie within the uncertainties of the experimental constraints, the spectra of light and medium nuclei show clear structures associated to η' -nuclear bound states and to threshold enhancements in the unbound region.

PACS numbers: 21.85.+d; 21.65.Jk; 25.80.-e

I. INTRODUCTION

The η' meson is an important particle to understand QCD dynamics since it is linked to the $U_A(1)$ axial vector anomaly [1–5]. Yet, the $\eta' N$ interaction is poorly known. Experimentally, one has estimates of the modulus of the scattering length, $|a_{\eta' N}| \sim 0.1$ fm [6]. The recent studies of the transparency ratio in η' photoproduction from nuclei indicate that the width $\Gamma_{\eta'}$ of the η' in the nucleus for momenta of the η' around 1050 MeV is about 20–30 MeV at nuclear saturation density, $\rho = \rho_0$ [7]. Yet, the stability of the transparency ratio as a function of the η' momentum, suggesting a relatively constant inelastic $\eta' N$ cross section, also indicates that $\Gamma_{\eta'} (\simeq v_{\eta'} \sigma \rho)$ should be smaller at lower energies and values around 10 MeV could be a reasonable estimate. On the other hand we are only aware of one theoretical calculation of the $\eta' N$ interaction [8]. This calculation is done within the chiral unitary approach with coupled channels, including the Weinberg-Tomozawa interaction which acts only on the octet of pseudoscalar mesons. This requires the use of the mixing angle of the octet and singlet to give the physical η and η' mesons, that is taken from Ref. [9]. In addition, one also uses the Lagrangian that couples the singlet meson to the baryons developed in Ref. [10]. The unknown strength of the singlet Lagrangian can be constrained from the value of the modulus of the scattering length, $|a_{\eta' N}|$, but then the sign of the scattering amplitude remains unknown. Yet, the study of Ref. [8] finds that the inelastic cross sections are rather independent on this parameter and the model makes clear predictions and sets bounds on the scattering amplitude.

The possible existence of η' bound states in nuclei has been investigated in the past [11–13] where the mass of the η' in the medium was estimated from arguments of chiral symmetry restoration. A reduction of the η' mass in the medium of about 100 MeV was obtained in [13] and, invoking a small imaginary part of the optical potential, relatively narrow bound states were predicted and reactions to eventually measure them were also suggested. The modification of the η' mass has also been studied using various effective lagrangians of the Nambu-Jona-Lasinio type [14–16] or within the quark-meson coupling model [17]. None of these works included an imaginary component of the η' optical potential accounting for the effect of inelastic channels or multinucleon absorption.

In the present work we use the model of Ref. [8] to derive the η' nucleus optical potential and investigate the possibility of obtaining η' bound states in nuclei. As discussed in Ref. [8], the coupling of the singlet meson to the baryons contributes mostly to the η' elastic channel and barely modifies the inelastic channels. This unique feature resembles that of the anomaly effects suggested in Ref. [13] using arguments of symmetry. Since the value of the singlet coupling is a free parameter of the theory, we can vary its strength up to values that simulate the scenario proposed in Ref. [13].

In addition to the optical potential obtained from the selfenergy at lowest order in the nuclear density, $t\rho$, we also calculate, using standard many body techniques, the second order density contributions which account for η' absorption by pairs of nucleons. We study several options and use the experimental constraints [6, 7] to obtain likely optical potentials with which we evaluate the bound states in different nuclei. Assuming the potential to be attractive, we find bound states of η' in most nuclei, with their corresponding widths, which should be taken into consideration in an eventual experimental search. With this study we aim at getting a deeper insight and new information on the properties of the $\eta'(958)$ meson in nuclei and on possible effects of the $U_A(1)$ anomaly with the partial restoration of chiral symmetry at finite density.

II. FORMALISM

The η' selfenergy in nuclear matter at lowest order in the density is given by

$$\Pi^{\text{1st}} = t\rho, \quad (1)$$

where t is the particle-nucleon scattering matrix. The optical potential is related to it by

$$V_{\text{opt}}^{\text{1st}} = \frac{\Pi^{\text{1st}}}{2\omega_{\eta'}} , \quad (2)$$

where $\omega_{\eta'}$ is the energy of η' .

In the present work, we evaluate the η' optical potential for a η' meson at rest ($\vec{p}_{\eta'} \sim 0$). We use the $\eta'N$ scattering amplitudes of [8] for different values of $a_{\eta'N}$. Since we are only interested in the case where the interaction is attractive, we take the values of t corresponding to $\text{Re}(a_{\eta'N})$ positive. In Table I we show the values of t for the $\eta'N \rightarrow \eta'N$ elastic amplitude and the $\eta'N \rightarrow \eta N$ transition amplitude, which will play some role in the absorption process.

α	$ a_{\eta'N} $ [fm]	$t_{\eta'p \rightarrow \eta'p} [10^{-2} \text{MeV}^{-1}]$	$t_{\eta'p \rightarrow \eta p} [10^{-2} \text{MeV}^{-1}]$
-0.126	0.075	$-0.932 - 0.249i$	$0.00843 + 0.666i$
-0.193	0.1	$-1.26 - 0.252i$	$-0.0152 + 0.670i$
-0.333	0.15	$-1.91 - 0.261i$	$-0.0615 + 0.678i$
-0.834	0.3	$-3.85 - 0.310i$	$-0.200 + 0.699i$
-1.79	0.5	$-6.43 - 0.430i$	$-0.385 + 0.724i$
-3.93	0.75	$-9.63 - 0.667i$	$-0.615 + 0.748i$
-9.67	1	$-12.9 - 1.01i$	$-0.849 + 0.767i$

TABLE I: Elastic amplitude $t_{\eta'p \rightarrow \eta'p}$ and transition amplitude $t_{\eta'p \rightarrow \eta p}$ at the $\eta'N$ threshold energy calculated by the model of Ref. [8]. The parameter α indicates the coupling strength of the singlet meson to the baryons defined in Ref. [8], and $|a_{\eta'N}|$ is the calculated modulus of the $\eta'N$ scattering length.

The second order potential is evaluated using the diagrams of Fig. 1, which account for the absorption of the η' meson by pairs of nucleons.

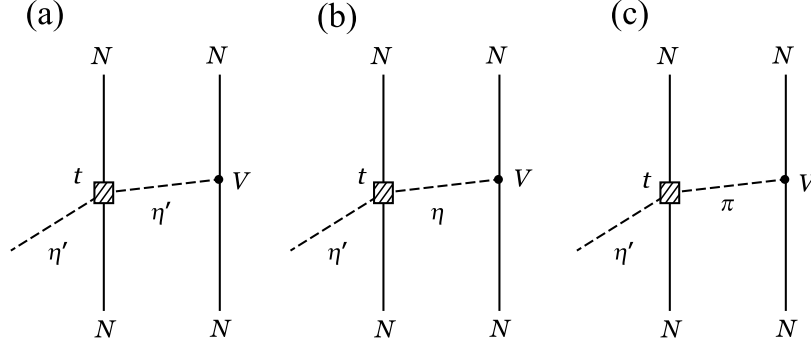


FIG. 1: Diagrams considered in the evaluation of the interaction of the η' meson with a pair of nucleons. The symbol t indicates the meson-nucleon scattering amplitude [8] and V the Yukawa vertex of each meson.

From these open diagrams we construct the many body diagrams of Fig. 2 for the η' selfenergy in nuclear matter. The imaginary part of the diagram of Fig. 2(a), stemming from the excitation of intermediate two-particle two-hole ($2p2h$) states, accounts for η' absorption by means of two nucleons, but there is also a source of imaginary part attached to the complex value of t . In addition, the diagrams also account for dispersive effects resulting in a real part of the η' selfenergy. These diagrams, involving two holes, have roughly a ρ^2 type behavior.

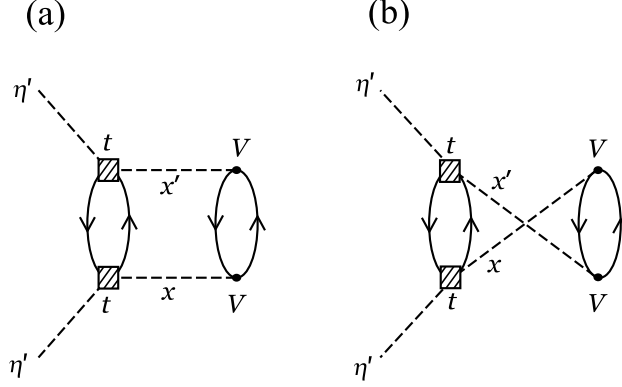


FIG. 2: Direct and crossed diagrams for the η' selfenergy in nuclear matter at second order. The symbols t and V indicate the scattering amplitude [8] and the Yukawa vertex as in Fig. 1. x and x' indicate the intermediate mesons.

The evaluation of the diagrams of Fig. 2 requires the knowledge of the t matrix for the $\eta'N \rightarrow \eta'N$, $\eta'N \rightarrow \eta N$ and $\eta'N \rightarrow \pi N$ transitions. Yet, the $\eta'N \rightarrow \pi N$ amplitude was found extremely small in [8], and experimentally the $\pi^- p \rightarrow \eta' n$ cross section is known to be of the order of 0.1 mb [18]. This is substantially smaller than the values of order of a few mb found for $\eta'N \rightarrow \eta'N$ or $\eta'N \rightarrow \eta N$ reactions in [8], in spite of the larger phase space involved in the $\eta'N \rightarrow \pi N$ transition. This allows us to neglect the diagram (c) in Fig. 1 and consider only the exchange of η' and η mesons in Fig. 2.

For the Yukawa vertex we use the standard Lagrangian as,

$$\mathcal{L}_{\text{Yukawa}} = \frac{D+F}{2f_\pi}(-\sqrt{2})\langle \bar{B}\gamma^\mu\gamma_5\partial_\mu\phi B \rangle + \frac{D-F}{2f_\pi}(-\sqrt{2})\langle \bar{B}\gamma^\mu\gamma_5 B\partial_\mu\phi \rangle. \quad (3)$$

The coupling of the η' is implemented adding to the SU(3) matrix of the pseudoscalar fields, ϕ , the term $\text{diag}(\eta_1, \eta_1, \eta_1)/\sqrt{3}$. We find the couplings for the octet and the singlet isospin zero pseudoscalar mesons as,

$$\mathcal{L}^8 = \frac{1}{\sqrt{3}} \frac{D-3F}{2f_\pi} \bar{p}\gamma^\mu\gamma_5 p \partial_\mu \eta_8, \quad (4)$$

$$\mathcal{L}^1 = -\sqrt{\frac{2}{3}} \frac{D}{f_\pi} \bar{p}\gamma^\mu\gamma_5 p \partial_\mu \eta_1. \quad (5)$$

Nonrelativistically this leads to two vertex functions of the type $V\vec{\sigma} \cdot \vec{q}$, with $V_\eta, V_{\eta'}$ given by

$$V_\eta = \cos\theta_P V_8 - \sin\theta_P V_1, \quad (6)$$

$$V_{\eta'} = \sin\theta_P V_8 + \cos\theta_P V_1, \quad (7)$$

where θ_P is the η_1 - η_8 mixing angle, for which we take the value 14.34° of Ref. [9], and

$$V_8 = \frac{1}{\sqrt{3}} \frac{3F-D}{2f_\pi}, \quad (8)$$

$$V_1 = \sqrt{\frac{2}{3}} \frac{D}{f_\pi}, \quad (9)$$

with $F=0.465$, $D=0.795$ [19]. The relativistic calculation with the γ_5 operators can be done by simply substituting \vec{q}^2 by the relativistic $-q^2$.

Following standard many-body techniques, the second order η' selfenergy, $\Pi^{2\text{nd}}$, depicted in Fig. 2 is obtained from

$$-i\Pi^{2\text{nd}}(p_{\eta'}) = \sum_{x,x'=\eta,\eta'} \int \frac{d^4q}{(2\pi)^4} iU(p_{\eta'} - q) iU(q) (-it_{\eta'N \rightarrow xN}) (-it_{x'N \rightarrow \eta'N}) \\ \times \frac{i}{q^2 - m_x^2 + i\epsilon} \frac{i}{q^2 - m_{x'}^2 + i\epsilon} V_x V_{x'} q^2, \quad (10)$$

where the indices x and x' express the intermediate η and/or η' mesons and $U(k)$ is the Lindhard function corresponding to a particle-hole (ph) excitation defined as,

$$U(k) = 4 \int \frac{d^3p}{(2\pi)^3} \frac{M}{E(\vec{p})} \frac{M}{E(\vec{k} + \vec{p})} \left[\frac{n(\vec{p})(1 - n(\vec{p} + \vec{k}))}{k^0 + E(\vec{p}) - E(\vec{p} + \vec{k}) + i\epsilon} + \frac{n(\vec{p} + \vec{k})(1 - n(\vec{p}))}{-k^0 + E(\vec{p} + \vec{k}) - E(\vec{p}) + i\epsilon} \right], \quad (11)$$

with the factor 4 accounting for the sum over the nucleon spin and isospin. Here, the first term in the integral corresponds to the direct diagram while the second term corresponds to the crossed diagram of the fermion loop of the ph excitation. In the present calculation, we find that the contribution of the crossed diagram in the first Lindhard function $U(p_{\eta'} - q)$ of Eq. (10) is small and can be neglected safely. As for the second Lindhard function $U(q)$ of Eq. (10), we include both direct and crossed terms in Eq. (11). Hence, the second order selfenergy of η' calculated here by Eq. (10) consists of the contributions shown in Fig. 2 (a) and (b). We use average values of \vec{p}^2 and \vec{p} to replace $E(\vec{p})$ and $E(\vec{p} + \vec{k})$ in the denominator of Eq. (11) as,

$$E(\vec{p}) \rightarrow E_F = \sqrt{M_N^2 + 3k_F^2/5} \quad (12)$$

$$E(\vec{p} + \vec{k}) \rightarrow E(\vec{k}) \quad (13)$$

where k_F is the Fermi momentum defined as,

$$\frac{2k_F^3}{3\pi^2} = \rho(r). \quad (14)$$

We also use the same average value for the occupation number $n(\vec{p} + \vec{k})$ in the numerator in Eq. (11) as,

$$n(\vec{p} + \vec{k}) \rightarrow n(\vec{k}). \quad (15)$$

Together with these approximations, we can perform the d^3p integration by using the relation,

$$4 \int \frac{d^3p}{(2\pi)^3} n(\vec{p}) = \rho, \quad (16)$$

and we finally get

$$-i\Pi^{2\text{nd}}(p_{\eta'}) = - \sum_{x,x'=\eta,\eta'} \int \frac{d^4q}{(2\pi)^4} \rho^2 \left(\frac{M}{E(\vec{q})} \right)^2 (1 - n(\vec{q})) t_{\eta'N \rightarrow xN} t_{x'N \rightarrow \eta'N} V_x V_{x'} q^2 \\ \times \frac{1}{p_{\eta'}^0 - q^0 + E_F - E(\vec{q}) + i\epsilon} \left[\frac{1}{q^0 + E_F - E(\vec{q}) + i\epsilon} + \frac{1}{-q^0 + E_F - E(\vec{q}) + i\epsilon} \right] \\ \times \frac{1}{q^2 - m_x^2 + i\epsilon} \frac{1}{q^2 - m_{x'}^2 + i\epsilon}, \quad (17)$$

where we have taken $M/E_F \sim 1$. Performing the q^0 integration using Cauchy theorem and summing up the contributions of all poles, we obtain a simplified expression of the η' self-energy $\Pi^{2\text{nd}}(p_{\eta'})$ which is calculated numerically. The second order optical potential $V_{\text{opt}}^{2\text{nd}}$ is obtained as $V_{\text{opt}}^{2\text{nd}} = \Pi^{2\text{nd}}/2\omega_{\eta'}$.

In order to obtain the optical potential in finite nuclei we use the local density approximation, substituting ρ by $\rho(r)$, where $\rho(r)$ is assumed to be an empirical Woods-Saxon form. This prescription was proved to be exact for s -wave [20], which is the only one we consider here.

III. RESULTS

In Table II, we show the numerical results of the optical potential V_{opt} at normal nuclear matter density $\rho = \rho_0$ for different values of the scattering length $a_{\eta'N}$ corresponding to those of Table I. We find that the strength of the optical potential at normal nuclear density is $V_{\text{opt}}|_{\rho_0} = -(8.71 + 1.82i)$ MeV for the case $|a_{\eta'N}| = 0.1$ fm, which is consistent to the data in Ref. [6]. In the case with $|a_{\eta'N}| = 0.5$ fm, we have $V_{\text{opt}}|_{\rho_0} = -(45.14 + 5.47i)$ MeV, giving rise to a width $\Gamma = -2\text{Im}V_{\text{opt}} \sim 10$ MeV, which could be a reasonable extrapolation to low η' momentum values of the transparency ratio data of Ref. [7]. If we consider an extreme case with $|a_{\eta'N}| = 1$ fm, we obtain a deep potential with a relatively small imaginary part, $V_{\text{opt}}|_{\rho_0} = -(91.81 + 17.21i)$ MeV. The potential in this extreme case has similar features as the one discussed in Refs. [12, 13]; however, the corresponding scattering length is much larger than the experimental value reported in Ref. [6].

	potential depth at $\rho = 0.17 \text{ fm}^{-3}$		bound states : $n\ell$ (B.E., Γ) [MeV]	
$ a_{\eta'N} $ [fm]	$V_{\text{opt}}^{1\text{st}}$ [MeV]	$V_{\text{opt}}^{2\text{nd}}$ [MeV]	^{11}C	^{39}Ca
0.075	$-6.36 - 1.70i$	$-0.07 - 0.05i$	- -	- -
0.1	$-8.61 - 1.72i$	$-0.10 - 0.10i$	- -	$0s$ $(-1.61, 2.01)$
0.15	$-13.04 - 1.78i$	$-0.19 - 0.23i$	- -	$0s$ $(-4.51, 2.78)$
0.3	$-26.26 - 2.11i$	$-0.56 - 0.91i$	$0s$ $(-4.65, 2.55)$	$0s$ $(-15.33, 5.09)$ $0p$ $(-5.43, 3.74)$
0.5	$-43.83 - 2.93i$	$-1.31 - 2.54i$	$0s$ $(-14.50, 5.95)$	$0s$ $(-31.79, 10.05)$ $1s$ $(-4.29, 5.16)$ $0p$ $(-18.94, 8.38)$
0.75	$-65.62 - 4.55i$	$-2.57 - 5.73i$	$0s$ $(-29.34, 12.80)$ $0p$ $(-7.22, 7.52)$	$0s$ $(-53.91, 20.14)$ $1s$ $(-18.70, 13.70)$ $0p$ $(-38.44, 17.60)$ $1p$ $(-3.06, 8.61)$
1	$-87.72 - 6.86i$	$-4.09 - 10.35i$	$0s$ $(-46.10, 23.34)$ $1s$ $(-0.29, 4.99)$ $0p$ $(-18.73, 15.78)$	$0s$ $(-77.65, 35.42)$ $1s$ $(-36.58, 26.34)$ $0p$ $(-59.96, 31.66)$ $1p$ $(-16.33, 20.56)$

TABLE II: Numerical results of the optical potential strength at normal nuclear density and results of the η' -nucleus bound states in ^{11}C and ^{39}Ca are shown for various $|a_{\eta'N}|$ values. The strengths of the lowest order ($V_{\text{opt}}^{1\text{st}}$) and the second order ($V_{\text{opt}}^{2\text{nd}}$) potentials are listed separately.

As we can see, for values of $|a_{\eta'N}|$ of the order of 0.1 fm, the second order potential is smaller than the first one, but for values of $|a_{\eta'N}|$ of the order of 0.5 fm the imaginary part of the second

order potential acquires a value comparable in size to that of the first order contribution. If we take a value of $|a_{\eta'N}|$ of the order of 1 fm, the imaginary part of the second order potential is 50% larger than the one of lowest order, which indicates the breakdown of the low-density expansion and that absorption by more nucleons may start being sizable. Since the imaginary part from additional multinucleon absorption processes not considered here will always be negative, we expect the imaginary part of the self-energy to be larger than the present results for the $|a_{\eta'N}| \gtrsim 0.5$ fm cases.

We solve the Klein-Gordon equation and look for bound states with V_{opt} for different nuclei. The results are shown in Table II for ^{11}C and ^{39}Ca . We find η' bound states in ^{11}C for $|a_{\eta'N}| \gtrsim 0.3$ fm and in ^{39}Ca for $|a_{\eta'N}| \gtrsim 0.1$ fm. The level spacings of the bound states are smaller than the widths for some cases as shown in Table II. Thus, there would be a possibility to observe these states experimentally.

As an example, by using the the same theoretical model of Refs. [21, 22], we calculate theoretically the expected formation cross section of the η' bound states in the (π^+, p) reaction at the pion beam momentum $p_\pi = 1.8$ GeV/c, which can be available at the J-PARC facility. We consider the forward reactions where the emitted proton is observed at 0 degrees in the laboratory frame to reduce the momentum transfer. The momentum transfer, however, is larger than 200 MeV/c even at the forward angle and cannot be zero at any kinematics in this reaction. The cross section for this reaction is evaluated using the Green's function method [23] in which we solve the Klein-Gordon equation both for the bound and unbound η' meson with the η' optical potential. The pion and proton wave functions are also distorted using the eikonal approximation. The neutron in the target nucleus is assumed to be described by a simple harmonic oscillator wavefunction. The energy of the emitted proton determines the energy of the η' -nucleus system uniquely. We show the calculated spectra in Figs. 3 and 4 as functions of the excitation energy $E_{\text{ex}} - E_0$ defined as

$$E_{\text{ex}} - E_0 = -B_{\eta'} + [S_n(j_n) - S_n(\text{ground})], \quad (18)$$

where $B_{\eta'}$ is the η' binding energy and $S_n(j_n)$ the neutron separation energy from the neutron single-particle level j_n . $S_n(\text{ground})$ indicates the separation energy from the neutron level corresponding to the ground state of the daughter nucleus. E_0 is the η' production threshold energy. In Figs. 3, 4(a) and 4(b), we find that a clear peak structure appears. The result with the deep potential shown in Fig. 4(c) has similar features as those found in Ref. [22]. We also show the spectrum for the repulsive potential case in Fig. 4(a), where we assume an opposite (repulsive) sign for $\text{Re}(V_{\text{opt}})$ in the $|a_{\eta'N}| = 0.3$ fm case. The spectra for nuclei heavier than ^{39}Ca have an overlap of different $[n\text{-hole} \otimes \eta']$ configurations that smear out the individual peaks and would not be suited for experimental searches.

The results shown in Figs. 3 and 4 deserve some comments. The peaks appearing in the most bound region correspond to a situation where the neutron has been removed from the less bound orbit, namely $(0d_{3/2})_n$ for the ^{40}Ca target (Fig. 3) and $(0p_{3/2})_n$ for the ^{12}C target (Fig. 4), and the η' is in the most bound $0s$ state. The final nucleus is thus left in its ground state which is stable. We also take into account situations where the neutron has been taken from an inner orbit, leaving a hole in the final nucleus which is then in a particular excited state. These states decay and their width is tied to the imaginary part of the nucleon nucleus potential for energies below the Fermi energy [24–26]. The widths of the hole states are taken into account in the present calculation. The width of the neutron-hole states in ^{39}Ca have been estimated to be $\Gamma = 7.7$ MeV $((1s_{1/2})^{-1})$, 3.7 MeV $((0d_{5/2})^{-1})$, 21.6 MeV $((0p_{3/2,1/2})^{-1})$, and 30.6 MeV $((0s_{1/2})^{-1})$ from the data in Ref. [27], considering the width of the ground state $(0d_{3/2})^{-1}$ to be 0 and assuming the same widths for neutron-hole states as those of proton holes. As for ^{11}C , we have used the data in Ref. [28] and the widths are $\Gamma((0s_{1/2})^{-1}) = 12.1$ MeV for the excited state and $\Gamma((0p_{3/2})^{-1}) = 0$ MeV for the ground state. The first and second peaks from the left in the total spectrum for the ^{40}Ca target,

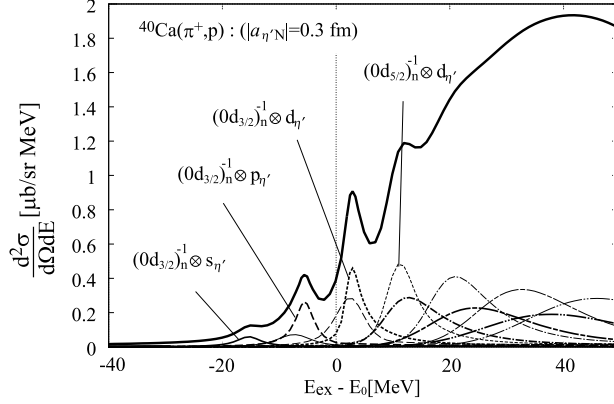


FIG. 3: Calculated spectra of $\eta'(958)$ mesic nuclei formation in the (π^+, p) reaction on a ^{40}Ca target at $p_\pi = 1.8$ GeV/c for the case $|a_{\eta'N}| = 0.3$ fm, as functions of the excitation energy $E_{\text{ex}} - E_0$, where E_0 is the η' production threshold energy. The total spectrum is shown by the thick solid line, and the dominant $[n\text{-hole} \otimes \eta']$ configurations are also shown in the figures. The neutron-hole states are indicated as $(n\ell_j)_n^{-1}$ and the η' states as $\ell_{\eta'}$. The elementary cross section is estimated to be $100 \mu\text{b/sr}$ in the laboratory frame [18, 22].

shown in Fig. 3, correspond to cases in which the neutron is removed from the outermost single-particle orbit $((0d_{3/2})_n)$ and the η' is left bound in the daughter nucleus ^{39}Ca in the lower s and p states, respectively. The third peak just above the threshold ($E_{\text{ex}} - E_0 = 0$) is dominated by an unbound d -wave component of the η' accompanied by the removal of the outer neutron. While there are no bound d states of η' in this case, as can be seen in the results shown in Table II, the attractive η' -nucleus interaction pulls this low energy scattering wave of the η' closer to the daughter nucleus enhancing its overlap with the nucleon wavefunctions and consequently producing a larger cross section. This is the so-called threshold enhancement of the quasi-elastic (unbound) η' contributions around the production threshold. Therefore, we can consider this enhancement to give an indication of the attractive η' -nucleus interaction if it is observed. The fourth peak from the left at $E_{\text{ex}} - E_0 \sim 12$ MeV has the same origin as the third peak of the threshold enhancement, except that it is accompanied by the removal of the inner neutron state $(0d_{5/2})_n$. Extra peaks in the higher energy region have the same interpretation but correspond to the higher angular momentum partial waves.

We can observe that in an intermediate mass nucleus like ^{40}Ca , the capture of the η' in the most bound $(0s)$ state with removal of an outer nucleon, produces a peak with too small strength, diluted with the tail from other states, which would not be suited for experimental observation. The production of a $0p$ η' state, however, leads to a distinct signal. In the case of a lighter nucleus like ^{12}C , a peak in the bound region can be observed, as long as $|a_{\eta'N}|$ does not differ too much from the value where it starts producing bound states (see the upper and middle panels of Fig. 4). Curiously, it does not help to have a larger strength for the optical potential (lower panel in Fig. 4). Indeed, the peaks corresponding to the production of the η' in the most bound state have small strength and are diluted due to the overlap of competing contributions from the removal of nucleon states from inner and wider orbits. Only a feeble signal over a large background stands up in the bound region corresponding to the production of the η' in the $0p$ bound state with the removal of the outer nucleon.

An interesting observation of the numerical results for attractive potentials is the robustness of the appearance of the peak structures in the spectra around the meson production threshold, in contrast to the spectrum calculated with the repulsive potential, where we only find a smooth quasifree contribution without any peak structure, as shown in Fig. 4(a). The origin of the struc-

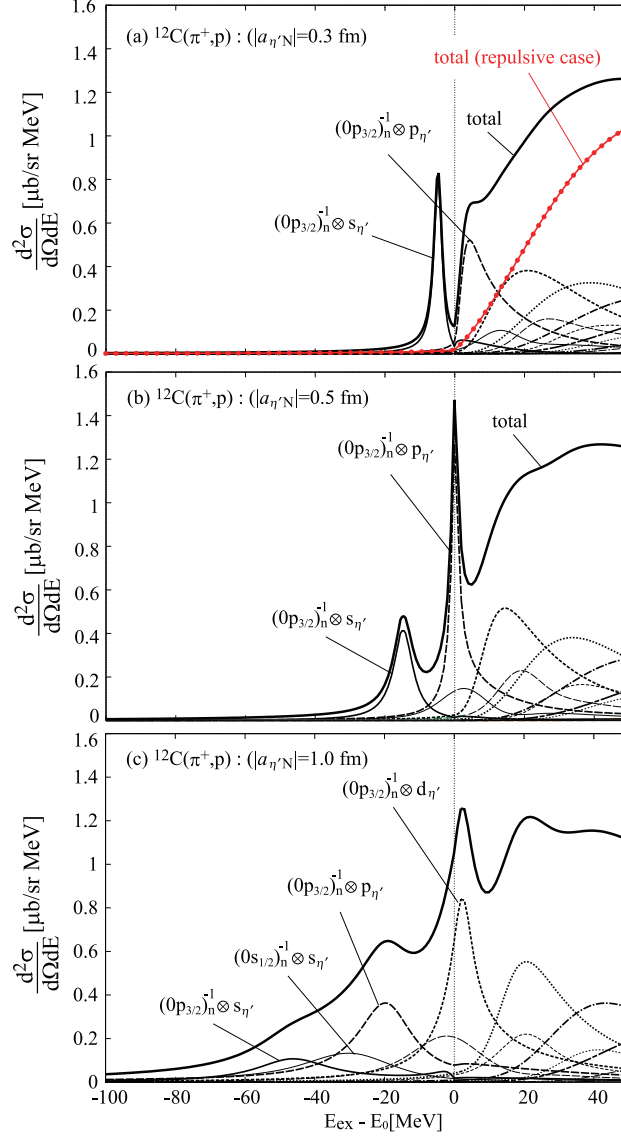


FIG. 4: (color online) Calculated spectra of $\eta'(958)$ mesic nuclei formation in the (π^+, p) reaction on a ^{12}C target at $p_\pi = 1.8$ GeV/c for the (a) $|a_{\eta'N}| = 0.3$ fm, (b) $|a_{\eta'N}| = 0.5$ fm, and (c) $|a_{\eta'N}| = 1.0$ fm cases, as functions of the excitation energy $E_{\text{ex}} - E_0$, where E_0 is the η' production threshold energy. The potential is assumed to be attractive as explained in the text. The total spectra are shown by the thick solid lines, and the dominant [n-hole $\otimes\eta'$] configurations are also shown in the figures. The total spectrum for the repulsive potential case is also shown for $|a_{\eta'N}| = 0.3$ fm in panel (a) by the solid circles with the thin line. The neutron-hole states are indicated as $(n\ell_j)_n^{-1}$ and the η' states as $\ell_{\eta'}$. The elementary cross section is estimated to be $100 \mu\text{b/sr}$ in the laboratory frame [18, 22].

tures depend on the target nucleus and the η' -nucleus potential strength, and they can be associated to genuine η' bound states and/or to an enhancement of the quasifree contribution. In any case, they give an indication of the attractive feature of the potential and can provide new information on the properties of the η' meson in nuclei. The robustness of the appearance of structures for an attractive interaction, which is independent on the details of the theory, could be helpful for actual experiments even if subsequent more refined measurements might be required to properly identify the origin of the peak structure in the spectrum.

In summary, we have observed that, depending on the strength of the potential, some nuclei

are better suited than others to eventually find peaks that can be identified with the production of possible bound η' states in nuclei. The calculated spectra shown in Figs. 3 and 4 also indicate the experimental resolution needed to observe those peaks. We note that the relatively small width of these states has made the appearance of clean peaks possible, in contrast with the situation with \bar{K} mesons in nuclei where the widths are very large [29–31].

IV. CONCLUSIONS

We have done a calculation of the η' -nucleus optical potential, starting from the lowest order term in the nuclear density and adding the second order term which accounts for η' absorption by pairs of nucleons. The strength of the potential is unknown, because of the limitations of the theory, where one has a free parameter tied to the coupling of the singlet of mesons to the baryons, for which the only constraint is the poorly known $\eta'N$ scattering length. At present, we can not even predict the sign, so we cannot claim the existence of bound η' states in nuclei. However, the free parameter of the theory is related to the $\eta'N$ scattering length and, assuming different values for it, we have obtained η' -nucleus potentials with varying strength that produced bound states in several nuclei. The potential strength can be made similar to that expected in Refs. [12, 13], but it requires a very large scattering length value of $|a_{\eta'N}| \simeq 1$ fm in the present calculation. One welcome feature of the theory is that, within a wide range of values of the scattering length, the imaginary part of the potential is reasonably smaller than the real part and this leads to bound η' states with a width smaller than the separation between the levels. In such cases, one may in principle expect to see distinguishable peaks in some experiments.

As an example of a possible experiment we have presented results for the (π^+, p) reaction, which can be measured at J-PARC, complementary to the reaction investigated in [32] at ELSA. We note that (π^-, n) reactions on isospin symmetric targets as the ones used here, ^{12}C and ^{40}Ca , would have given similar η' production spectra. Given the fact that there is a proposal at J-PARC that plans to use this reaction to look for ω bound states [33] measuring forward going neutrons, the results that we get would be useful if this reaction is also done to look for η' states. In the photoproduction case, we can naively expect to obtain similar spectral shapes as shown in this paper with a smaller magnitude of the formation cross section, of order of 5–10 nb/sr/MeV [11, 12].

We found that, for certain values of the scattering length and some nuclei, clean peaks could be resolved. The bound state peaks are visible in light or medium nuclei and correspond to situations where the potential is not too deep. The peaks appear at binding energies smaller than 20 MeV and their widths are of the order of 10 MeV. This certainly requires having a good experimental resolution. It is also interesting to observe that the structure of the spectrum around threshold gives clear indications about the character (attractive or repulsive) of the η' -nucleus interaction. In the present situation, where not even the sign of the scattering length, and hence of the η' -nucleus potential, is known, an experiment searching for bound η' in nuclei, either producing positive or negative results, would provide a welcome information on the properties of the elementary $\eta'N$ interaction, putting constraints on the size of the scattering length and eventually determining its unknown sign.

Acknowledgments

We appreciate the useful comments by V. Metag and M. Nanova. This work is partly supported by projects FIS2006-03438, FIS2008-01661 from the Ministerio de Ciencia e Innovación (Spain), by the Generalitat Valenciana in the program Prometeo and by the Generalitat de Catalunya contract 2009SGR-1289. This work is also supported by the Grant-in-Aid for Scientific Research

(No. 22105510 and No. 20540273) in Japan. This research is part of the European Community-Research Infrastructure Integrating Activity “Study of Strongly Interacting Matter” (acronym HadronPhysics2, Grant Agreement n. 227431) and of the EU Human Resources and Mobility Activity “FLAVIANet” (contract number MRTN-CT-2006-035482), under the Seventh Framework Programme of EU.

-
- [1] J. B. Kogut and L. Susskind, Phys. Rev. D **10**, 3468 (1974).
 - [2] S. Weinberg, Phys. Rev. D **11**, 3583 (1975).
 - [3] G. 't Hooft, Phys. Rev. Lett. **37**, 8 (1976).
 - [4] E. Witten, Nucl. Phys. B **149**, 285 (1979).
 - [5] K. Kawarabayashi and N. Ohta, Nucl. Phys. B **175** (1980) 477.
 - [6] P. Moskal *et al.*, Phys. Lett. B **482**, 356 (2000) [arXiv:nucl-ex/0004006].
 - [7] M. Nanova *et al.*, to appear in Proceedings of the XIV International Conference on Hadron Spectroscopy, HADRON2011, June 13-17, 2011, München (Germany).
 - [8] E. Oset, A. Ramos, Phys. Lett. **B704**, 334-342 (2011). [arXiv:1010.5603 [nucl-th]].
 - [9] F. Ambrosino, A. Antonelli, M. Antonelli, F. Archilli, P. Beltrame, G. Bencivenni, S. Bertolucci, C. Bini *et al.*, JHEP **0907**, 105 (2009). [arXiv:0906.3819 [hep-ph]].
 - [10] B. Borasoy, Phys. Rev. **D61**, 014011 (2000). [hep-ph/0001102].
 - [11] H. Nagahiro, S. Hirenzaki, Phys. Rev. Lett. **94**, 232503 (2005). [hep-ph/0412072].
 - [12] H. Nagahiro, M. Takizawa, S. Hirenzaki, Phys. Rev. **C74**, 045203 (2006). [nucl-th/0606052].
 - [13] D. Jido, H. Nagahiro, S. Hirenzaki, [arXiv:1109.0394 [nucl-th]].
 - [14] V. Bernard, U. G. Meissner, Phys. Rev. **D38** (1988) 1551.
 - [15] T. Kunihiro, Phys. Lett. **B219** (1989) 363-368.
 - [16] P. Costa, M. C. Ruivo, Yu. L. Kalinovsky, Phys. Lett. **B560** (2003) 171-177. [hep-ph/0211203].
 - [17] K. Tsushima, Nucl. Phys. A **670** (2000) 198c-201c.
 - [18] R. K. Rader, M. A. Abolins, O. I. Dahl, J. S. Danburg, D. W. Davies, P. L. Hoch, J. Kirz, D. H. Miller, Phys. Rev. **D6**, 3059-3068 (1972).
 - [19] B. Borasoy, Phys. Rev. **D59**, 054021 (1999). [hep-ph/9811411].
 - [20] J. Nieves, E. Oset, C. Garcia-Recio, Nucl. Phys. **A554**, 509-553 (1993).
 - [21] H. Nagahiro, D. Jido, S. Hirenzaki, Phys. Rev. **C80** (2009) 025205. [arXiv:0811.4516 [nucl-th]].
 - [22] H. Nagahiro, Prog. Theor. Phys. Suppl. **186** (2010) 316-324.
 - [23] O. Morimatsu, K. Yazaki, Nucl. Phys. **A435** (1985) 727-737; O. Morimatsu, K. Yazaki, Nucl. Phys. **A483** (1988) 493-513.
 - [24] C. Mahaux, P. F. Bortignon, R. A. Broglia, C. H. Dasso, Phys. Rept. **120**, 1-274 (1985).
 - [25] P. Fernandez de Cordoba, E. Oset, Phys. Rev. **C46**, 1697-1709 (1992).
 - [26] S. Fantoni, B. L. Friman, V. R. Pandharipande, Nucl. Phys. **A399**, 51-65 (1983).
 - [27] K. Nakamura, S. Hiramatsu, T. Kamae, H. Muramatsu, N. Izutsu, Y. Watase, Phys. Rev. Lett. **33** (1974) 853-855.
 - [28] S. L. Belostotskii, S. S. Volkov, A. A. Voribev, Yu. V. Dotsenko, L. G. Kudhin, N. P. Kuropatkin, O. V. Miklukho, V. N. Nikulin, and O. E. Prokofev, Sov. J. Nucl. Phys. **41** (6), 903 (1985).
 - [29] A. Ramos, E. Oset, Nucl. Phys. **A671**, 481-502 (2000). [nucl-th/9906016].
 - [30] J. Schaffner-Bielich, V. Koch and M. Effenberger, Nucl. Phys. A **669**, 153 (2000) [arXiv:nucl-th/9907095].
 - [31] S. Hirenzaki, Y. Okumura, H. Toki, E. Oset, A. Ramos, Phys. Rev. **C61**, 055205 (2000).
 - [32] M. Nanova, private communication.
 - [33] K. Ozawa *et al.*, "Direct measurements of ω mass modification in $A(\pi^-, n)\omega$ reaction and $\omega \rightarrow \pi^0\gamma$ decays", Proposal for J-PARC (2010), http://j-parc.jp/NuclPart/pac_1007/pdf/KEK_J-PARC-PAC2010-08.pdf